JACS
JOURNAL OF THE AMERICAN CHEMICAL SOCIETY
Article
pubs.acs.org/JACS

Thiolated DNA-Based Chemistry and Control in the Structure and Optical Properties of Plasmonic Nanoparticles with Ultrasmall Interior Nanogap

Jeong-Wook Oh,[†] Dong-Kwon Lim,[‡] Gyeong-Hwan Kim,[†] Yung Doug Suh,*[,§] and Jwa-Min Nam*[,†]

[†]Department of Chemistry, Seoul National University, Seoul 151-747, South Korea

[‡]Department of BIN Fusion Technology, Chonbuk National University, Jeonju 561-756, South Korea

[§]Laboratory for Advanced Molecular Probing (LAMP), Research Center for Convergence Nanotechnology, Korea Research Institute of Chemical Technology, Daejeon 305-600, South Korea

Supporting Information

ABSTRACT: The design, synthesis and control of plasmonic nanostructures, especially with ultrasmall plasmonically coupled nanogap (~1 nm or smaller), are of significant interest and importance in chemistry, nanoscience, materials science, optics and nanobiotechnology. Here, we studied and established the thiolated DNA-based synthetic principles and methods in forming and controlling Au core-nanogap-Au shell structures [Au-nanobridged nanogap particles (Au-NNPs)] with various interior nanogap and Au shell structures. We found that differences in the binding affinities and modes among four different bases to Au core, DNA sequence, DNA grafting density and chemical reagents alter Au shell growth mechanism and interior nanogap-forming process on thiolated DNA-modified Au core. Importantly, poly A or poly C sequence creates a wider interior nanogap with a smoother Au shell, while poly T sequence results in a narrower interstitial interior gap with rougher Au shell, and on the basis of the electromagnetic field calculation and experimental results, we unraveled the relationships between the width of the interior plasmonic nanogap, Au shell structure, electromagnetic field and surface-enhanced Raman scattering. These principles and findings shown in this paper offer the fundamental basis for the thiolated DNA-based chemistry in forming and controlling metal nanostructures with ~1 nm plasmonic gap and insight in the optical properties of the plasmonic NNPs, and these plasmonic nanogap structures are useful as strong and controllable optical signal-generating nanoprobes.

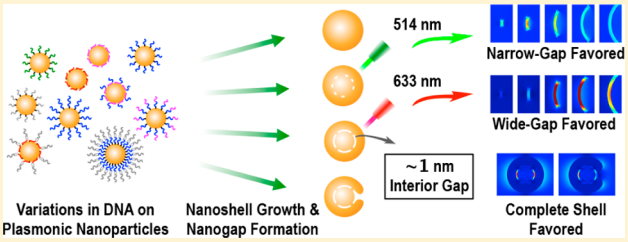

INTRODUCTION

Plasmonic nanostructures such as Au and Ag nanoparticles (AuNPs and AgNPs) have been of great interest in many scientific and engineering disciplines, and their plasmonically coupled and localized regions, "hot spots", have been heavily studied for their intense optical properties.[1−3] Typically, these hot spots are formed within plamonic gap between or inside metal nanostructures, and they can generate extraordinarily enhanced optical properties that are useful in various applications including nanoantenna[4,5] and surface-enhanced Raman scattering (SERS).[1,6−8] It is particularly important to form ~1 nm plasmonic gap because this ultrasmall plasmonic nanogap offers much larger signal enhancement and more narrow distribution of SERS enhancement factor values than >1 nm plasmonic gap nanostructures.[7,9] For these reasons, it is highly beneficial to develop strategies for synthesizing, controlling and utilizing plasmonic nanostructures with ~1 nm nanogap. Although many different strategies to fabricate plasmonic nanostructures have been reported,[10−24] synthesizing targeted plasmonic nanostructures with ultrasmall nanogap in high precision and high yield is still an important challenge to address for maximizing the signal intensity from the nanostructure and minimizing variation in signal intensity between nanostructures. In particular, on-wire lithography is a powerful approach that combines the template-directed synthesis of nanowires with the chemical etching process for the formation of nanogap,[25] and this method allows for the straightforward control of the size and the position of nanogap in anisotropic nanorods. However, generating ultrasmall (~1 nm) nanogaps and obtaining highly reproducible optical signals from different nanogap structures still remain challenging with this approach.

Recently, we reported the formation of interior ~1 nm gap inside AuNPs while growing Au shell on thiolated DNA-modified Au cores, and remarkably high synthetic yield (~95%) for these Au-nanobridged nanogap particles (Au-NNPs) was observed.[26] Highly uniform and strong SERS signals [SERS enhancement factor (EF) was $>10^8$, and most particles generated EF values within $\sim10^8-10^9$ range] from these particles were observed and analyzed with the atomic force microscopy-correlated nano-Raman measurements for particle-

Received: April 29, 2014
Published: September 8, 2014

   dx.doi.org/10.1021/ja504270d | J. Am. Chem. Soc. 2014, 136, 14052−14059

by-particle analysis. However, no synthetic mechanism and nanogap-controlling strategies for the ∼1 nm interior gap nanoparticles have been shown nor proposed in the previous report, and only one specific thiolated DNA sequence was used therein. Methods for controlling structure-dependent plasmonic signals from these structures have not been studied, and the principles for plasmonic signal enhancement for the Au-NNPs have not been systematically explored. These studies are critical for the understanding and general use of this thiolated DNA-based plasmonic nanogap-forming chemistry inside particles, and unraveling the synthetic chemical principles for this can open revenues for new synthetic chemistry for nanomaterials with ultrasmall interior gap. And, we also need to study and derive the relationship between Au-NNP structure and optical signal for the better understanding and use of these structures in chemical and biological sensing and imaging applications.[27−29]

Here, we established the thiolated DNA-based chemistry in forming plasmonic particles with ultrasmall interior nanogap and the principles of optical signal enhancement in generating strong, quantifiable and controllable plasmonic signals from these nanogap structures. To figure out how AuNP surface-modified thiolated DNA affects the formation of the interior nanogap, we varied DNA base, length, sequence, grafting density, etc., and their corresponding optical properties (e.g., electromagnetic field and SERS) have been analyzed. We found different interior nanogap structures were formed when different thiolated DNA sequences were used, and four different DNA sequences (poly A, poly T, poly G and poly C) generated different nanogap and Au shell structures, mainly because of different binding affinities and modes between different DNA bases and AuNP core surface.[30−34] By using various thiolated DNA sequences and observing and analyzing Au shell growth and interior nanogap formation, we established the chemistry of ∼1 nm gap formation inside AuNPs. Importantly, different Au-NNP structures with different nanogap widths can be formed by controlling the interactions between thiolated DNA bases and Au core, and the Au-NNP structures with relatively wider nanogap generated stronger SERS signal with 633 nm excitation laser than 514 nm laser while the Au-NNPs with relatively narrower nanogap generated stronger SERS signal with 514 nm excitation source than 633 nm laser. Furthermore, we also found out that DNA grafting density on Au core is important in controlling Au shell formation and nanogap structures and generating strong and stable signals from Au-NNPs. Finally, based on these findings, we were able to establish the relationships between thiolated DNA sequence, DNA grafting density, Au-NNP structure and corresponding plasmonic optical signals such as electromagnetic (EM) field and SERS, which provide the fundamental basis for the designed synthesis of the interior nanostructures and the use of these structures for the plasmonically enhanced signal-based detection and imaging applications.

EXPERIMENTAL SECTION

Materials. All the chemical reagents [$HAuCl_4{\cdot}3H_2O$, poly-*N*-vinyl-2-pyrrolidone (PVP, MW 40 000), hydroxylamine hydrochloride, dithiothreitol (DTT), mercaptopropanol and sodium dodecyl sulfate (SDS) and sodium chloride] were purchased from Sigma-Aldrich (St. Louis, MO, USA) and used without further purification. Gold nanoparticles (AuNPs) were purchased from BBInternational (UK). HPLC-purified thiolated oligonucleotides were purchased from IDT Inc. (Coralville, IA, USA) and reduced by using 0.1 M DTT in the phosphate-buffered solution (0.17 M, pH = 8.0). The reduced oligonucleotides were then purified through disposable NAP-5 columns (Sephadex G-25 medium, DNA grade), which were purchased from GE Healthcare. NANOpure H_2O (>18.0 MΩ, Milli-Q) was used for all the experiments. The Formvar/carbon-coated copper grids (Ted Pella, Inc. Redding, CA, USA) were used for the TEM analysis (JEM-2100, JEOL, at NCIRF).

Synthesis of Au-NNPs. DNA-modified AuNPs were synthesized with salt-aging steps based on literature procedures.[7,15,26] Thiolated poly A, poly C, poly G and poly T are 3′-HS-$(CH_2)_3$-(Cy3)-A_{10}-5′, 3′-HS-$(CH_2)_3$-(Cy3)-C_{10}-5′, 3′-HS-$(CH_2)_3$-(Cy3)-G_{10}-5′, and 3′-HS-$(CH_2)_3$-(Cy3)-T_{10}-5′, respectively. In the cases of the extended forms in Figure 5 and Figure S2 (Supporting Information, SI), 3′-PEG_{18}-AAA CTC TTT GCG CAC-5′ was added to 5′ position of the above A_{10} and T_{10} sequences. Briefly, thiolated oligonucleotides were reduced by 0.1 M dithiothreitol (DTT) in 0.17 M PBS solution (pH 8.0) and then purified with a desalting NAP-5 column. 145 μL of freshly purified oligonucleotides (20 μM), which is corresponding to 5000-fold number of AuNP particles, were added to 500 μL of 20 nm AuNP solution (O.D. = 1.0) with 0.01% SDS and then mixed with 100 mM phosphate buffer (PB), pH 7.4, to adjust to obtain the final concentration of 10 mM PB solution. The mixture solution was incubated with mild shaking for 1 h. The resulting solution was adjusted to the final concentration of NaCl by adding the aliquots of 2 M NaCl (10 mM PB, 0.01% SDS) solution. After the addition of each aliquot to result in the increment of 50 mM NaCl concentration for each addition step, the mixture was kept with mild shaking at 70 °C for 20 min. After the salt-aging step, the mixture solution was incubated at room temperature with mild shaking overnight. The solution was then centrifuged (12 000 rpm) for 15 min, the supernatant was removed carefully and the precipitate was redispersed in DI water (this procedure was repeated two times). To control the grafting density of immobilized DNA, the final salt concentration during the salt-aging step was varied. The loading number of thiolated DNAs per nanoparticle was quantified by measuring the fluorescence signal of Cy3 dye-conjugated to DNAs after releasing immobilized DNAs on AuNPs through excess DTT treatment.[35] Before the formation of Au shell, 100 μL of the diluted DNA-modified AuNP solution (O.D. = 0.5) was mixed with 50 μL of 1% PVP and then the mixed solution was adjusted to the final concentration of 0.15 M PBS (pH 7.4) solution with 100 mM PB and 2 M NaCl solution, respectively. Au shell was formed after 10 mM hydroxylamine and 5 mM $HAuCl_4$ (the amount of each solution was adjusted to determine Au shell thickness) were sequentially added to the resulting DNA-modified AuNP with vigorous stirring for 90 s. The solution was kept standing for 1 h and then followed by the centrifugation and redispersion in DI water before the Raman spectrum measurement. Raman spectra were acquired in solution using the Renishaw inVia setup, equipped with Leica optical microscope [20× objective lens (NA 0.40) with 514 and 633 nm laser excitation sources (10 mW laser power, 10 s integration time)]. The Raman intensity of each sample was averaged three different positions in solution, and Renishaw WiRE 3.2 software was used for data acquisition and analysis.

Quenching Au Shell Formation Process with Mercaptopropanol. To quench the Au shell growth process, we added 40 μL of 30 mM mercaptopropanol to each Au shell growing solution with vigorous stirring immediately at 2, 3, 5, and 20 s after adding the Au precursors. After a few minutes when the quenching reaction was completed, we measured the UV−vis spectrum of each case and obtained TEM images.

3D Finite-Element-Method-Based Electromagnetic Field Calculation. We calculated the electromagnetic field distributions of various Au-NNP structures with the 3D finite-element-method (FEM). The interior nanogap was formed between Au core and Au shell and designed by two different ways. In the first case, the interior gap was formed by cutting the convex-typed cylindrical space with 1.2 nm height above the surface of Au core. The size of the interior gap was controlled by the angular length between the terminal sides of a hollow interior gap, which corresponds to the length of the curved arc. The other case is that four interior cylindrical nanobridges with 2.5 nm (diameter) × 1.2 nm (height) dimensions were constructed between

dx.doi.org/10.1021/ja504270d | J. Am. Chem. Soc. 2014, 136, 14052−14059

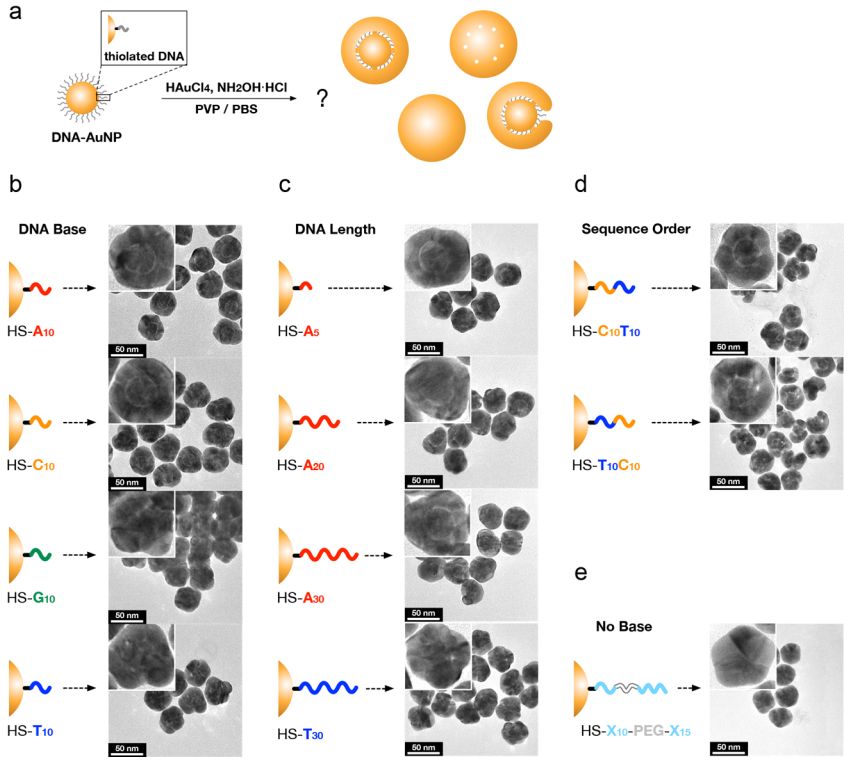

Figure 1. Thiolated DNA-based chemistry in forming plasmonic nanoparticles with ultrasmall interior nanogap. (a) Schematic diagram for the synthesis of Au nanogap particles. (b–d) Thiolated DNA sequences and the corresponding transmission electron microscopic (TEM) images of Au nanostructures after Au shell formation on Au core. Thiolated DNA strands were varied in DNA base species (b), length (c), and sequence order (d). (e) Thiolated DNA without DNA bases and the TEM image of the resulting nanostructures. All the scale bars in the TEM images are 50 nm.

Au core and Au shell. The former model was fit to compare the interior gap size, which is shown in Figure 2 while the latter model was fit to compare the complete shell to the incomplete shell, which is shown in Figures 4 and 5. The core diameter was 20 nm, and the shell thickness was 11 or 15 nm. The more details on the calculation can be found in ref 26.

RESULTS AND DISCUSSION

Roles of DNA Sequence in Synthesizing Au-NNP Structures. First, we systematically designed a variety of thiolated DNA sequences while varying DNA base, length and sequence order or removing DNA bases to understand the roles of DNA in forming plasmonic nanogap particle structures (Figure 1). In a typical experiment, thiolated DNA strands were modified to citrate-stabilized 20 nm AuNPs in 50 mM PBS solution (please see the Experimental Section for details; thiol group was modified at 3′ end for all the DNA sequences). After purifying DNA-modified AuNPs (DNA-AuNPs), Au-NNPs were formed from DNA-AuNP cores in PBS solution with PVP as a stabilizer and the reduction of $HAuCl_4$ with hydroxylamine as a mild reducing agent. As a first variation in DNA, we introduced four different DNA sequences (HS-A_{10}, HS-C_{10}, HS-G_{10} and HS-T_{10}) to find out how the resulting Au-NNP structures were affected by different DNA bases. It should be noticed that A is the strongest binder to Au surface while T is the weakest binder to Au surface.[30−34] In the cases of HS-A_{10} and HS-C_{10} sequences, uniform and wide ∼1 nm nanogaps were formed for nearly all the particles (Figure 1b), and their corresponding UV−vis spectra were very similar to each other as shown in Figure S1 (SI). In the case of HS-G_{10}, small nanohole-like gaps were formed, and many aggregate particles were observed, possibly due to the chemical instability of G bases and the formation of G-quadruplex of poly G sequences, as shown in the TEM image and UV−vis absorption spectrum (Figure 1b and S1 (SI)).[36,37] Thiolated T_{10}-modified Au cores generated popcorn-like Au shell structures, and irregularly shaped narrow nanogaps were formed (Figure 1b). These bumpy Au shell surface and irregular nanohole shapes resulted in the slight red-shift and broadening in the UV−vis spectrum (Figure 1b and S1 (SI)). The results substantiate the binding affinity of DNA bases to Au surface is important in forming the interior plasmonic gap inside Au nanoparticles as relatively strong Au surface binders, poly A and poly C, induce uniform and wide nanogap with smoother Au shell surface while the weakest Au surface binder, poly T, generates irregular nanohole-type gaps with popcorn-like Au shell structures.

We then varied DNA length and studied the effect of DNA length on the interior nanogap formation (Figure 1c). For both poly A and poly T cases, our results suggest that change in DNA length does not have significant effect on the interior nanogap and Au shell formation. A_5, A_{10}, A_{20} and A_{30} cases generated very similar structures with similar interior nanogap features, and T_{10} and T_{30} resulted in very similar Au-NNP structures with the nearly identical spectral data. When the order of two linked sequences was switched, however, there is a clear difference in the resulting Au-NNP structures (Figure 1d; please notice that a set of $A_{10}T_{10}$ and $T_{10}A_{10}$ was not used here due to the possibility of self-hybridization or hairpin structure formation). The case for HS-$C_{10}T_{10}$ generated the Au-NNP structures that are more similar to HS-C_{10} case while HS-$T_{10}C_{10}$ generated the Au-NNP structures that are closer to the structures from HS-T_{10} case. The results indicate that the DNA sequence that is close to thiol-Au bond (inner sequence) dominantly controls the resulting Au-NNP structures while the

dx.doi.org/10.1021/ja504270d | J. Am. Chem. Soc. 2014, 136, 14052−14059

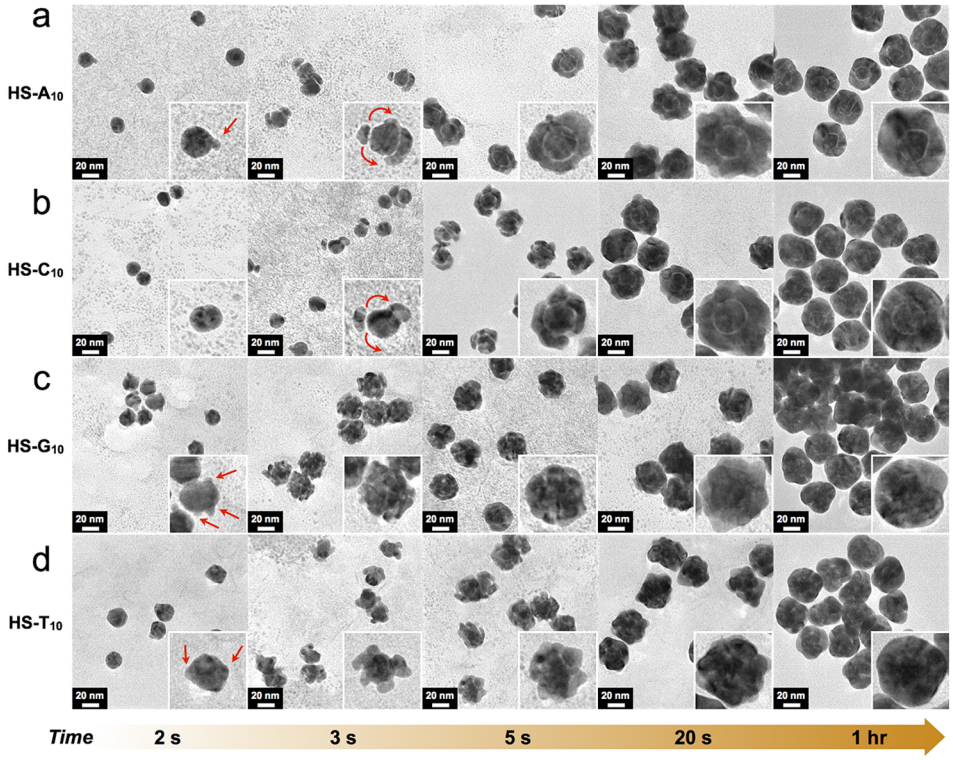

Figure 2. Snapshots of DNA-dependent Au shell and interior gap formation processes on Au core. (a–d) TEM images of intermediates prepared by quenching the Au shell growth reaction with mecrcaptopropanol at 2, 3, 5, and 20 s after the reaction was initiated. The TEM images in (a), (b), (c), and (d) are the quenched nanoparticle images from HS-A_{10}, HS-C_{10}, HS-G_{10} and HS-T_{10}-modified AuNPs, respectively.

sequence that is far from Au surface (outer sequence) play less significant role in Au-NNP structure formation. We also extended DNA sequence by inserting PEG and additional sequence, but the resulting Au-NNP structures were similar to the cases without PEG and additional sequence (Figure S2 (SI)). Finally, we removed DNA bases from DNA structures while leaving sugar moiety, phosphate backbone and thiol group within a thiolated DNA structure and formed Au shell on base-less DNA-modified Au core. No interior gap was formed in this case, and the results conclusively show that it is critical to have DNA bases that interact with Au core surface to form the interior gap (Figure 1e).

Synthetic Mechanism for the Formation of Au-NNP Structures. Next, we analyzed the interior nanogap forming chemistry with time-lapse snapshot-based TEM image analysis while varying DNA bases (poly A, poly T, poly G and poly C). The images of intermediate structures were obtained by quenching the Au-NNP growth process using the formation of Au(I)-thiol complex with excess mecrcaptopropanol.[16] As shown in Figure 2a–d, the nucleation processes with small budding structures on Au cores were observed, and different Au budding patterns were observed from different thiolated DNA sequences. Budding Au structures were formed on Au core surface for the first a few seconds, and these budding Au nanostructures were then connected and smoothened to form Au shell and interior nanogap. Overall, for HS-A_{10} and HS-C_{10}-modified AuNP core cases, very few budding sites were observed for each Au core and Au shell was formed via the lateral shell growth from the budding sites to form the uniform and wide interior gap while HS-G_{10} and HS-T_{10}-modified AuNP cores generated multiple Au budding sites on a Au core and interstitial interior gaps were formed from multiple budding Au structures. One can readily notice that HS-G_{10}-modified AuNP cores induced particle aggregations and these structures are not appropriate for controllable and quantifiable SERS signal generation. For this reason, thiolated poly G-modified AuNP cores and corresponding thiolated poly G-induced Au-NNP structures were not further studied for SERS applications.

It is known that adenine (A) and cytosine (C) have a relatively strong binding affinity to Au surface, while thymine (T) has the weakest binding affinity to Au surface.[31,33,34] For this reason, the numbers of modified HS-A_{10} and HS-C_{10} per AuNP were smaller than that of HS-T_{10} (see Figure S3 (SI)).[31,33] From a structural viewpoint of DNA, large part of poly A or poly C that is close to Au surface is bound to Au surface while poly T is more densely packed on Au surface and more vertically stretched out due to their weaker binding nature to Au surface. The effective Au core surface coverage by HS-A_{10} or HS-C_{10} should be larger than that of HS-T_{10} due to a myriad of direct interactions between poly A or poly C bases and Au core surface. Larger Au core surface area could be protected by Au-surface-binding poly A or poly C than more weakly binding poly T, and these intimate bindings between DNA bases and Au surface could effectively protect Au core surface from Au precursors (e.g., $AuCl_4^-$, $[AuCl_x(OH)_{4-x}]^-$; the component ratio is dependent on pH[38]) to prevent direct Au shell formation on Au core surface without forming the interior gap. In contrast, HS-T_{10} modified AuNP cores induced multiple nucleation sites and multiple budding Au structures, giving rise to smaller and narrower interstitial nanogaps, rather than uniform, laterally wide gap, between AuNP core and Au shell. One can also recognize that the thickness of single-stranded DNA is ~1 nm, and this is another supporting evidence that

dx.doi.org/10.1021/ja504270d | J. Am. Chem. Soc. 2014, 136, 14052–14059

the interior gap is formed between Au core and shell due to the binding between DNA bases and Au core surface. The UV−vis spectra and solution colors that correspond to each growth step of each case further support the above trends; thiolated poly A and thiolated poly C cases share lots of similarity in Au-NNP structures and corresponding optical properties, while thiolated poly T case induced broader spectrum and more darker solution color (Figure S4 (SI)).

Thiolated DNA Sequence and Excitation Laser Wavelength-Dependent SERS Signals from Au-NNPs. Using the synthesized Au-NNP structures, we show that the differently formed Au-NNP structures, based on different DNA sequences, generate different SERS signals. When Cy3-modified thiolated DNA (HS-Cy3-DNA sequence) was modified to Au cores, Cy3 dyes can be positioned in the interior nanogap after Au shell formation, and we tested three different thiolated oligonucleotides (HS-Cy3-A_{10}, HS-Cy3-C_{10}, and HS-Cy3-T_{10}; Figure 3). 514 and 633 nm laser sources were

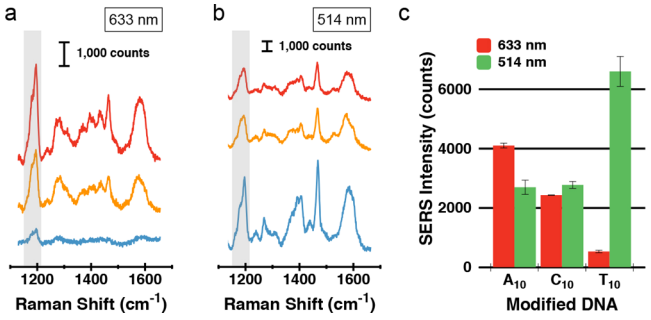

Figure 3. SERS spectra of Cy3 dyes in Au-NNP structures. (a,b) The representative SERS spectra were taken from 0.30 nM Au-NNP solution for Au-NNPs with HS-Cy3-A_{10} (red), HS-Cy3-C_{10} (orange), and HS-Cy3-T_{10} (blue), respectively. (c) The quantitative comparison of SERS intensities at 1194 cm^{-1} from different Au-NNPs. Error bars for the SERS signals came from three different positions on the same Au-NNP solution.

used as incident excitation sources because it was reported that different excitation laser sources can result in different SERS intensities.[26] Among the characteristic peaks for Cy3 dye (1194, 1466, and 1580 cm^{-1}), the SERS signal intensity at 1194 cm^{-1} was chosen as the representative signal for the quantitative comparison between different cases. As shown in Figure 3c, 633 nm source generated the strongest SERS signal with thiolated poly A while the strongest SERS signal was obtained from thiolated poly T case with 514 nm excitation source. It should be noticed that the number of modified DNA strands per Au-NNP is significantly different among poly A and poly T cases (Figure S3a (SI)). Considering this effect, the difference in SERS signal between poly A and poly T in the case of 633 nm laser is even larger than as appeared in Figure 3c and Figure S3b (SI). It should be pointed out that highly enhanced SERS signal with 514 nm wavelength is very unusual in Au nanostructures due to the presence of interband transitions at ~500 nm.[39,40] Such increase of SERS signal with 514 nm incident light is thought to be mainly due to the surface-enhanced resonance Raman scattering (SERRS) effect considering the absorbance spectrum of Cy3 (there are two absorbance peaks at 515 and 548 nm in Cy3-modified DNA). The results clearly show that one can tune the SERS signals from Au-NNPs by controlling Au-NNP structures with different thiolated DNA sequences.

Relationships between the Width of the Interior Nanogap and Electromagnetic Field. To systematically study how change in the interior gap width effect on the EM field enhancement and distribution inside Au-NNP, we performed a theoretical calculation with a three-dimensional finite-element method (FEM) (COMSOL Multiphysics). The thicknesses of the interior gap and Au shell with 20 nm Au core were fixed to be 1.2 and 11 nm, respectively (Figure 4a), and

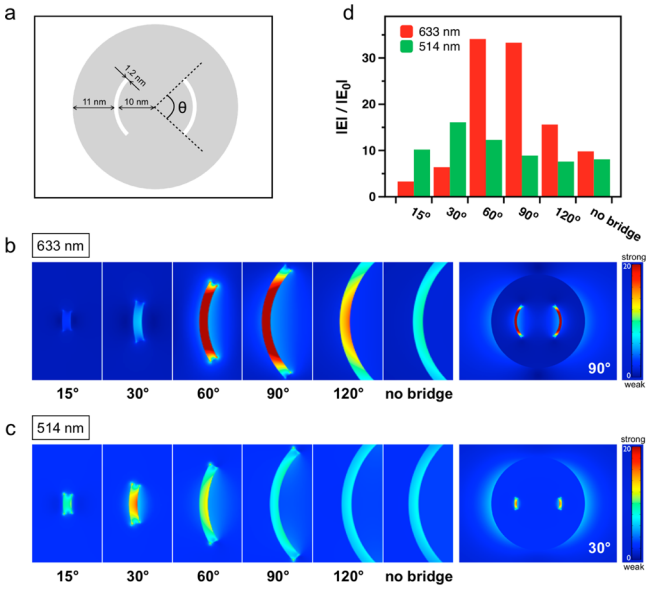

Figure 4. Calculated electromagnetic (EM) field distributions of the Au-NNPs with varying the interior nanogap widths. (a) A diagram depicts the arc angle of the interior nanogap, θ, the vertical thickness of the interior gap (1.2 nm), Au core size (20 nm) and Au shell thickness (11 nm). (b,c) Simulated near-field EM field distribution inside the Au core-gap-Au shell structure at an incident laser wavelength of (b) 633 nm or (c) 514 nm while varying the interior gap angle from 15° to 120°. The far-right images in (b) and (c) are the entire EM field views of the Au-NNPs with the largest field enhancement in the interior gap (90° arc nanogap for 633 nm excitation for (b) and 30° arc nanogap for 514 nm excitation for (c)). (d) Comparison in the EM field enhancements with the varying arc nanogap widths and incident wavelengths.

the arc angle of the interior gap (θ) was gradually widened from 15° to 120° (Figure 4b and 4c). First, 633 nm laser was applied in the FEM calculation because 633 nm is a more resonant excitation source with the EM field of Au nanostructure than 514 nm excitation source, which is competed with the interband transition at ~500 nm.[39,40] Typically, it is known that the surface plasmon resonance (SPR) signal is strongly enhanced within a highly localized small hot spot, but our results suggest that the EM field in the most narrow interior gap (15° gap in Figure 4b) was revealed as the weakest EM field generator among Au-NNPs with 633 nm incident light. The largest increase in the EM field in the interior gap was observed at 60° and 90° for 633 nm incident wavelength. As the angle of the interior gap gets wider than 90°, the EM field intensity declines quickly. Interestingly, although it was shown the nanobridges that connect Au core and shell are important not only for generating the hollow interior gap but also enhancing the EM field inside Au-NNPs, the EM field in the interior gap without the nanobridges is stronger than those with very small interior gaps (15° and 30° gaps) in this case (Figure

dx.doi.org/10.1021/ja504270d | J. Am. Chem. Soc. 2014, 136, 14052−14059

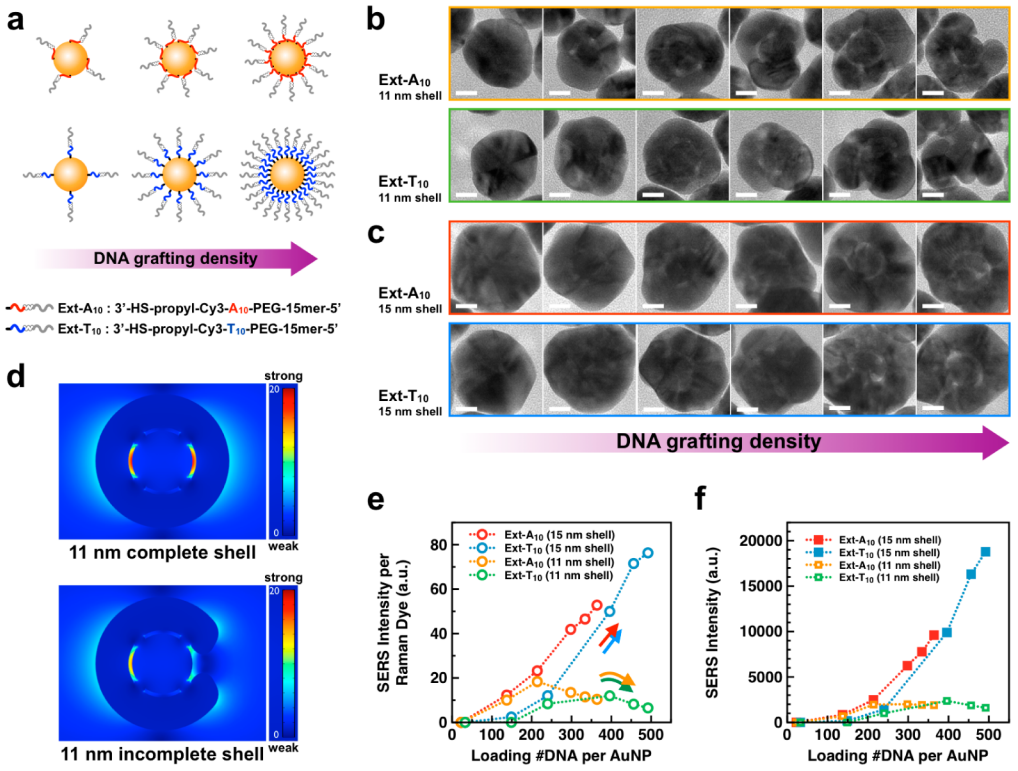

Figure 5. DNA grafting density-dependent interior gap formation and corresponding electromagnetic fields and SERS signals. (a) Schematic diagram of DNA grafting density effect on the formation of Au shell and interior nanogap. (b,c) Representative TEM images of Au nanostructures for 11 nm Au shell (b) or 15 nm Au shell (c) with varying DNA grafting densities on 20 nm Au core (from left to right, in H_2O, 10 mM PB, 50 mM PBS, 300 mM PBS, 500 mM PBS and 700 mM PBS solutions, respectively). Scale bar = 10 nm. (d) Comparison of the EM fields between complete 11 nm Au shell and incomplete 11 nm Au shell at an incident wavelength of 633 nm. (e) The normalized SERS intensities from the Au-NNPs with varying amounts of loaded DNA per AuNP and two different Au shell thicknesses. All the data points in the graph correspond to the Au nanostructures in (b) and (c) (from left to right). (f) SERS intensities from Au-NNPs in the same particle concentration before normalization in (e).

4b and 4d). The results suggest that arc gap angle and nanobridges need to be simultaneously considered in controlling and understanding the plamonic signal from Au-NNP structures. Overall tendency shown here with 633 nm laser can explain why the 633 nm incident light-based SERS intensity of HS-A_{10} or HS-C_{10}-modified Au-NNPs with the wider interior gap is stronger than that of HS-T_{10}-modified Au-NNPs with the narrower interior nanogap.

When 514 nm incident light was used, overall, the EM field intensity was decreased and the tendency is different from 633 nm laser case (Figure 4c). Importantly, the strongest EM field inside Au-NNP was obtained from the Au-NNP with 30° arc gap. This trend matches well with the experimental SERS results for HS-T_{10}-generated Au-NNP where much stronger SERS signal was observed from the Au-NNPs with more narrow interior gaps than the Au-NNPs with wider gaps when 514 nm excitation source was used (Figure 3c). The EM field intensities in 15° and 30° interior gaps with 514 nm incident light were 3.1 and 2.5-fold stronger, respectively, than those with 633 nm laser. On the contrary, the EM field intensities in wider-angle gap cases (60° and 90°) with 514 nm laser generated 2.8 and 3.7-fold weaker signals than the results with 633 nm excitation source. It should be noticed that there is always discrepancy for the quantitative comparison between theoretical and experimental results from Au-NNPs because, although our synthetic strategy generates relatively uniform Au-NNPs, there are always structural heterogeneity among formed nanostructures and micro-Raman experimental SERS data are based on ensemble average results from many particles.

Effect of DNA Grafting Density on the Structure and SERS Signal of Au-NNP. Finally, we controlled the number of modified DNA strands per particle because our results suggest that DNA density could affect the Au-NNP structures and corresponding SERS signals. For the investigation of DNA grafting density effect with different DNA sequences, we used extended sequences as 3′-HS-A_{10}-PEG-AAA CTC TTT GCG CAC-5′ (ext-A_{10}) and 3′-HS-T_{10}-PEG-AAA CTC TTT GCG CAC-5′ (ext-T_{10}) sequences (Figure 5a). The reason why we chose the extended sequence with PEG and tailing oligonucleotides is due to the aggregation tendency of shorter thiolated oligonucleotide sequences during harsh salt-aging process for synthesizing DNA-modified AuNPs with a very high DNA grafting density. The DNA grafting density on an AuNP was controlled by varying salt-aging conditions (i.e., H_2O only, 10 mM PB without salt, 50, 300, 500, and 700 mM PBS conditions). The numbers of loaded DNAs per AuNP for 50, 300, 500, and 700 mM PBS conditions are 214, 298, 334, and 364 for ext-A_{10} and 240, 396, 456, and 492 for ext-T_{10}, respectively (Figure S5 (SI)). Figure 5b (11 nm Au shell) and 5c (15 nm Au shell) show the representative images of Au-NNP structures after the formation of Au shell with the varying DNA grafting densities (more images are shown in Figure S6 (SI)). Overall trend is that no interior gap was formed when DNA grafting density is low and more distinctive interior gap was formed with intermediate or high DNA grafting density cases. However, one can readily recognize incomplete shell structures were formed for very high grafting DNA density cases with 11 nm Au shell cases (Figure 5b). For very low DNA

dx.doi.org/10.1021/ja504270d | J. Am. Chem. Soc. 2014, 136, 14052−14059

grafting density cases, a small number of Au core surface-immobilized DNA strands did not effectively protect the surface from the reduction of Au precursors on AuNP core surface, resulting in the straightforward core−shell particle formation without interior nanogap. Contrarily, for very high DNA grafting density cases, a myriad of DNA strands can protect Au core surface much more effectively to generate incomplete Au shell as well as interior gap. The FEM calculation results suggest that the formation of complete Au shell is important to generate stronger and more uniform EM field inside Au-NNP (Figure 5d). For this reason, 15 nm Au shell cases are better in obtaining more completely closed shell structure around Au core with higher DNA grafting density than 11 nm Au shell cases, and the results suggest that completely closed Au shell structures from the Au core with densely modified DNA can be formed with 15 nm Au shell thickness (Figure 5c).

Next, we measured the SERS signals from the obtained nanostructures with varying DNA grafting densities and Au shell thicknesses (Figure 5e). For 11 nm Au shell cases, the SERS intensity increases only to a certain DNA grafting density level due to the incomplete Au shell formation on the Au core with densely modified thiolated DNA strands for both ext-A_{10} and ext-T_{10} (Figure 2b and 2e). On the other hand, 15 nm Au shell cases generated relatively larger SERS signals, and the difference between 15 and 11 nm Au shells in SERS intensity per Cy3 became dramatically larger when the number of loaded DNA strands per AuNP equals 298 or higher for ext-A_{10} case and 396 or higher for ext-T_{10} case (Figure 5e). The largest SERS signal per Cy3 dye was observed from ext-T_{10} case with 15 nm Au shell. When the SERS intensity per Au-NNP was considered, the signal was nearly 10-fold higher for ext-T_{10} with 15 nm Au shell than ext-A_{10} with 11 nm Au shell (Figure 5f). This shows it is important to modify the right DNA sequence with an optimized salting condition and Au shell thickness for obtaining the strongest SERS signals from Au-NNPs.

CONCLUSION

In summary, we have established the chemistry for designing and synthesizing plasmonic nanoparticles with ultrasmall (typically, ∼1 nm) interior gap using thiolated DNA and obtained the relationships between these metal nanogap structures and plasmonic signals from these structures. We found the bindings between DNA bases and AuNP surface and DNA grafting density on AuNP surface are critical in forming and controlling Au shell and plamonic interior gap inside Au-NNPs. Au shell formation and interior nanogap forming mechanism was also studied and analyzed, and all these provide useful chemical principles for the syntheses of various plasmonic nanogap materials and DNA-based nanostructures.[41,42] We also found the relationships between the width of the interior gap (the arc angle of the interior gap), excitation laser wavelength, EM field distribution inside Au-NNPs and SERS signal, which can offer the better understanding and fundamental basis for the use of these plasmonic nanogap structures for various applications and lead to the development of highly sensitive, quantitative and controllable optical signal-generating nanoprobes. We further expect that the synthetic principle described here can be used for other types of materials such as Ag and Pt and Au-NNPs can be applied to a variety of biomedical applications such as bioimaging, photothermal therapeutics and drug delivery.

ASSOCIATED CONTENT

Supporting Information

Six figures as described in the main text. This material is available free of charge via the Internet at http://pubs.acs.org.

AUTHOR INFORMATION

Corresponding Authors

jmnam@snu.ac.kr
ydsuh@krict.re.kr

Notes

The authors declare no competing financial interest.

ACKNOWLEDGMENTS

J.-M.N. was supported by the National Research Foundation (NRF) of Korea (2011-0018198) and BioNano Health-Guard Research Center funded by the Ministry of Science, ICT & Future Planning (MSIP) of Korea as Global Frontier Project (H- GUARD_2013M3A6B2078947). Y.D.S. acknowledges support from the Public Welfare & Safety Research Program (2011-0020957) through the National Research Foundation (NRF) funded by the Ministry of Science, ICT, and Future Planning (MSIP), Korea.

REFERENCES

(1) Halas, N. J.; Lal, S.; Chang, W.-S.; Link, S.; Nordlander, P. *Chem. Rev.* **2011**, *111*, 3913−3961.
(2) Willets, K. A. *ChemPhysChem* **2013**, *14*, 3186−3195.
(3) Kleinman, S. L.; Frontiera, R. R.; Henry, A.-I.; Dieringer, J. A.; Van Duyne, R. P. *Phys. Chem. Chem. Phys.* **2012**, *15*, 21.
(4) Giannini, V.; Fernández-Domínguez, A. I.; Heck, S. C.; Maier, S. A. *Chem. Rev.* **2011**, *111*, 3888−3912.
(5) Novotny, L.; van Hulst, N. *Nat. Photonics* **2011**, *5*, 83−90.
(6) Lim, D. K.; Jeon, K. S.; Kim, H. M.; Nam, J. M.; Suh, Y. D. *Nat. Mater.* **2010**, *9*, 60−67.
(7) Lee, J.-H.; Nam, J.-M.; Jeon, K.-S.; Lim, D.-K.; Kim, H.; Kwon, S.; Lee, H.; Suh, Y. D. *ACS Nano* **2012**, *6*, 9574−9584.
(8) McMahon, J. M.; Li, S.; Ausman, L. K.; Schatz, G. C. *J. Phys. Chem. C* **2011**, *116*, 1627−1637.
(9) Lee, H.; Lee, J.-H.; Jin, S. M.; Suh, Y. D.; Nam, J.-M. *Nano Lett.* **2013**, *13*, 6113−6121.
(10) Mirkin, C. A.; Letsinger, R. L.; Mucic, R. C.; Storhoff, J. J. *Nature* **1996**, *382*, 607−609.
(11) Alivisatos, A. P.; Johnsson, K. P.; Peng, X. G.; Wilson, T. E.; Loweth, C. J.; Bruchez, M. P.; Schultz, P. G. *Nature* **1996**, *382*, 609−611.
(12) Gandra, N.; Abbas, A.; Tian, L.; Singamaneni, S. *Nano Lett.* **2012**, *12*, 2645−2651.
(13) Liu, N.; Hentschel, M.; Weiss, T.; Alivisatos, A. P.; Giessen, H. *Science* **2011**, *332*, 1407−1410.
(14) Tan, S. J.; Campolongo, M. J.; Luo, D.; Cheng, W. *Nat. Nanotechnol.* **2011**, *6*, 268−276.
(15) Lee, J.-H.; Kim, G.-H.; Nam, J.-M. *J. Am. Chem. Soc.* **2012**, *134*, 5456−5459.
(16) Wang, Z.; Zhang, J.; Ekman, J. M.; Kenis, P. J. A.; Lu, Y. *Nano Lett.* **2010**, *10*, 1886−1891.
(17) Wang, Z.; Tang, L.; Tan, L. H.; Li, J.; Lu, Y. *Angew. Chem., Int. Ed.* **2012**, *51*, 9078−9082.
(18) Chen, G.; Wang, Y.; Yang, M.; Xu, J.; Goh, S. J.; Pan, M.; Chen, H. *J. Am. Chem. Soc.* **2010**, *132*, 3644−3645.
(19) Wang, Y.; Chen, G.; Yang, M.; Silber, G.; Xing, S.; Tan, L. H.; Wang, F.; Feng, Y.; Liu, X.; Li, S.; Chen, H. *Nat. Commun.* **2010**, *1*, 1−7.
(20) Urban, A. S.; Shen, X.; Wang, Y.; Large, N.; Wang, H.; Knight, M. W.; Nordlander, P.; Chen, H.; Halas, N. J. *Nano Lett.* **2013**, *13*, 4399−4403.
(21) Jin, Y.; Gao, X. *Nat. Nanotechnol.* **2009**, *4*, 571−576.

(22) Bardhan, R.; Mukherjee, S.; Mirin, N. A.; Levit, S. D.; Nordlander, P.; Halas, N. J. *J. Phys. Chem. C* **2010**, *114*, 7378−7383.
(23) Tao, A.; Sinsermsuksakul, P.; Yang, P. *Nat. Nanotechnol.* **2007**, *2*, 435−440.
(24) Henzie, J.; Andrews, S. C.; Ling, X. Y.; Li, Z.; Yang, P. *Proc. Natl. Acad. Sci. U. S. A.* **2013**, *110*, 6640−6645.
(25) Qin, L.; Park, S.; Huang, L.; Mirkin, C. A. *Science* **2005**, *309*, 113−115.
(26) Lim, D.-K.; Jeon, K.-S.; Hwang, J.-H.; Kim, H.; Kwon, S.; Suh, Y. D.; Nam, J.-M. *Nat. Nanotechnol.* **2011**, *6*, 452−460.
(27) Qian, X. M.; Nie, S. M. *Chem. Soc. Rev.* **2008**, *37*, 912.
(28) Le Ru, E. C.; Etchegoin, P. G. *Annu. Rev. Phys. Chem.* **2012**, *63*, 65−87.
(29) Ringe, E.; Sharma, B.; Henry, A.-I.; Marks, L. D.; Van Duyne, R. P. *Phys. Chem. Chem. Phys.* **2013**, *15*, 4110.
(30) Storhoff, J. J.; Elghanian, R.; Mirkin, C. A.; Letsinger, R. L. *Langmuir* **2002**, *18*, 6666−6670.
(31) Kimura-Suda, H.; Petrovykh, D. Y.; Tarlov, M. J.; Whitman, L. J. *J. Am. Chem. Soc.* **2003**, *125*, 9014−9015.
(32) Erdmann, M.; David, R.; Fornof, A. R.; Gaub, H. E. *Nat. Chem.* **2010**, *2*, 745−749.
(33) Brown, K. A.; Park, S.; Hamad-Schifferli, K. *J. Phys. Chem. C* **2008**, *112*, 7517−7521.
(34) Wang, F.; Liu, B.; Huang, P.-J. J.; Liu, J. *Anal. Chem.* **2013**, *85*, 12144−12151.
(35) Hurst, S. J.; Lytton-Jean, A. K. R.; Mirkin, C. A. *Anal. Chem.* **2006**, *78*, 8313−8318.
(36) Li, Z.; Mirkin, C. A. *J. Am. Chem. Soc.* **2005**, *127*, 11568−11569.
(37) Feng, D.-Q.; Liu, G.; Zheng, W.; Chen, T.; Li, D. *J. Mater. Chem. B* **2013**, *1*, 3057.
(38) Wang, S.; Qian, K.; Bi, X.; Huang, W. *J. Phys. Chem. C* **2009**, *113*, 6505−6510.
(39) Álvarez-Puebla, R. A. *J. Phys. Chem. Lett.* **2012**, *3*, 857−866.
(40) Ghosh, S. K.; Pal, T. *Chem. Rev.* **2007**, *107*, 4797−4862.
(41) You, M.; Peng, L.; Shao, N.; Zhang, L.; Qiu, L.; Cui, C.; Tan, W. *J. Am. Chem. Soc.* **2014**, *136*, 1256−1259.
(42) Xie, X.; Xu, W.; Liu, X. *Acc. Chem. Res.* **2012**, *45*, 1511−1520.